Applied Physics Letters

Controlling vertical magnetization shift by spin–orbit torque in ferromagnetic/antiferromagnetic/ferromagnetic heterostructure

Cite as: Appl. Phys. Lett. **116**, 062403 (2020); https://doi.org/10.1063/1.5139590
Submitted: 22 November 2019 . Accepted: 31 January 2020 . Published Online: 11 February 2020

Z. P. Zhou, X. H. Liu, and K. Y. Wang

View Online Export Citation CrossMark

ARTICLES YOU MAY BE INTERESTED IN

Interfacial Dzyaloshinskii-Moriya interaction between ferromagnetic insulator and heavy metal
Applied Physics Letters **116**, 052404 (2020); https://doi.org/10.1063/1.5134762

Epitaxially grown Cu_2Sb-type MnGaGe films with large perpendicular magnetic anisotropy
Applied Physics Letters **116**, 062402 (2020); https://doi.org/10.1063/1.5140398

Spin current propagation through ultra-thin insulating layers in multilayered ferromagnetic systems
Applied Physics Letters **116**, 042403 (2020); https://doi.org/10.1063/1.5119787

© 2020 Author(s).

Applied Physics Letters ARTICLE scitation.org/journal/apl

Controlling vertical magnetization shift by spin–orbit torque in ferromagnetic/antiferromagnetic/ferromagnetic heterostructure

Cite as: Appl. Phys. Lett. **116**, 062403 (2020); doi: 10.1063/1.5139590
Submitted: 22 November 2019 · Accepted: 31 January 2020 ·
Published Online: 11 February 2020

View Online Export Citation CrossMark

Z. P. Zhou,[1,2] X. H. Liu,[1,2,a)] and K. Y. Wang[1,2,3,4,a)]

AFFILIATIONS

[1]State Key Laboratory for Superlattices and Microstructures, Institute of Semiconductors, Chinese Academy of Sciences, Beijing 100083, China
[2]Center of Materials Science and Optoelectronics Engineering, University of Chinese Academy of Sciences, Beijing 100049, China
[3]Beijing Academy of Quantum Information Sciences, Beijing 100193, China
[4]Center for Excellence in Topological Quantum Computation, University of Chinese Academy of Science, Beijing 100049, China

[a)]**Author to whom correspondence should be addressed:** xionghualiu@semi.ac.cn and kywang@semi.ac.cn

ABSTRACT

We report the control of the vertical magnetization shift (VMS) and exchange bias through spin–orbit torque (SOT) in Pt/Co/$Ir_{25}Mn_{75}$/Co heterostructure devices. The exchange bias accompanying with a large relative VMS of about 30% is observed after applying a single pulse of 40 mA in a perpendicular field of 2 kOe. Furthermore, the field-free SOT-induced variations of VMS and exchange bias are also observed, which would be related to the effective built-in out-of-plane field due to unequal upward and downward interfacial spin populations. The SOT-induced switched fraction of out-of-plane interfacial spins shows a linear dependence on relative VMS, indicating that the number of uncompensated pinned spins is proportional to the switched interfacial spins. Our finding offers a comprehensive understanding for electrically manipulating interfacial spins of antiferromagnetic materials.

Published under license by AIP Publishing. https://doi.org/10.1063/1.5139590

Exchange bias (EB) refers to a shift in the hysteresis loop along the magnetic field axis due to the interface exchange coupling between ferromagnetic (FM) and antiferromagnetic (AFM) materials.[1–8] This phenomenon has been widely studied because of the technological application in spintronic devices and magnetic recording.[7] Furthermore, a vertical shift of FM magnetization is also observed in the FM/AFM system, which is claimed to be due to a number of frozen uncompensated or canting AFM spins at the FM/AFM interface.[9–14] Usually, the vertical magnetization shift (VMS) in the conventional FM/AFM system is quite small and cannot be easily detected by isothermal magnetization measurements, and most exchange bias models ignore the possibility of VMS.[15–17]

On the other hand, except for generating EB, AFM materials themselves have recently attracted tremendous attention due to their abundant properties for future spintronic applications: robustness against the external field, no stray fields, and ultrafast spin dynamics.[18,19] Remarkably, the discovery of electrical switching of an antiferromagnet by spin–orbit torque (SOT) motivates considerable research in AFM spintronics.[20–24] The magnetization switching caused by SOT commonly consists of a damping-like torque $\mathbf{m} \times (\boldsymbol{\sigma} \times \mathbf{m})$ and a field-like torque $\mathbf{m} \times \boldsymbol{\sigma}$, where $\mathbf{m}$ is the spin moment and $\boldsymbol{\sigma}$ is the spin polarization of spin current.[25,26] Besides the spin Hall effect (SHE), the Rashba effect, arising from the underlying crystal structure or interface inversion symmetry breaking, together with spin–orbit coupling also induces SOT switching.[25,26] To date, the manipulation of bulk properties of antiferromagnets has been realized by several different approaches,[18–24] and the tunability of EB through SOT was recently reported by Lin *et al.*[27] and Liu *et al.*[28] Furthermore, to explore the control of VMS via SOT will give a comprehensive understanding of electrically manipulating interfacial spins of AFM materials. To realize this aim, we design the device in heavy metal (HM)/FM/AFM/FM structures, where the bottom and top FM layers are perpendicular magnetic anisotropy (PMA) and in-plane anisotropy, respectively.[29]

In this work, we report the tunability of VMS and EB by SOT in the Pt(3)/Co(1)/$Ir_{25}Mn_{75}$(4)/Co(5) (thickness in nanometers) heterostructure. The current-induced EB with a large relative VMS of about 30% is observed. Moreover, we demonstrated the field-free SOT-induced modifications of VMS and EB. Our work provides a

Published under license by AIP Publishing

route to comprehensively understand the electrical control of AFM interfacial spins at the interface of AFM and FM.

The stack structure of Ta(1)/Pt(3)/Co(1)/$Ir_{25}Mn_{75}$(4)/Co(5)/Ta(2) (in nanometers) was deposited on a thermally oxidized Si substrate by magnetron sputtering at room temperature, as schematically illustrated in Fig. 1(a). Samples Ta(1)/Pt(3)/Co (1)/$Ir_{25}Mn_{75}$(4)/Ta(2) and Ta(1)/Pt(3)/Co(1.2)/$Ir_{25}Mn_{75}$(4)/Ru(3) without the top ferromagnetic layer and Ta(1)/Pt(3)/Co(1)/$Ir_{25}Mn_{75}$(4)/Co(5)/Al_2O_3(2) were studied as reference samples. The base pressure was less than 1×10^{-8} Torr before deposition, and the pressure of the sputtering chamber was 0.8 mTorr during deposition. No magnetic field was applied during the sputtering. The samples were then patterned into Hall bar devices with a channel width of 10 μm by photolithography and Ar-ion etching. The inset (up) of Fig. 1(b) shows the optical microscopy image of the Hall bar device. The measurements of magnetic and transport properties were performed at room temperature. All the R_H vs H_z loops were measured with a DC of 0.1 mA.

Figure 1(b) presents the anomalous Hall effect (AHE) resistance (R_H) dependence of the out-of-plane field ($H_z \perp$ film plane) for the Ta(1)/Pt(3)/Co(1)/$Ir_{25}Mn_{75}$(4)/Co(5)/Ta(2) device before applying the pulsed current, indicating that the 1 nm bottom Co layer exhibits PMA magnetization. Meanwhile, the two-step switching behavior, with a strong out-of-plane pinning due to the exchange coupling between Co(1)/$Ir_{25}Mn_{75}$(4) layers, is observed. The two-step hysteresis loops are associated with the occurrence of a bi-domain state, where the two domain populations are oppositely exchange biased because of opposite orientations of the uncompensated AFM spins at the FM/AFM interface.[30,31] The top Co layer has the magnetic easy axis in the plane [inset (down) of Fig. 1(b) with the H//film plane], and the small remanence is due to a weak in-plane exchange coupling between $Ir_{25}Mn_{75}$(4)/Co(5) layers.[2,3]

The Hall bar device was then subjected to a single current pulse I_p with a fixed width 50 ms, in a longitudinal field $H_x = 1$ kOe [inset (up) of Fig. 1(b)]. Through the spin Hall effect (SHE), a charge current in the $\pm$ **x** direction should produce a spin polarization along the $\pm$ **y** direction for the positive spin-Hall angle of Pt.[32–35] The resulting spin current can switch the magnetization of bottom PMA Co between the $\pm$ **z** directions, when both the current density and H_x are large enough. Moreover, the absorption of transverse spin currents is reported to vary with the FM thickness with a characteristic saturation length of 1.2 nm.[36] Thus, in our device, not only the 1 nm thick Co layer but also the AFM interfacial spins can be directly affected by SOT, leading to the variation of EB.[28] R_H vs H_z loops, obtained after applying single current pulses of $I_p = 40$ mA and -40 mA in $H_x = 1$ kOe, are shown in Figs. 1(c) and 1(d), respectively. In this process, first, we set $H_x = 1$ kOe and then applied a single pulse of $I_p = 40$ mA; after that, we set $H_x = 0$ and $I_p = 0$ and measured the R_H vs H_z loop. The R_H vs H_z loop for $I_p = -40$ mA under $H_x = 1$ kOe is obtained by using the same process. The main part of the loop shows positive EB for 40 mA [Fig. 1(c)] and negative EB for -40 mA [Fig. 1(d)], demonstrating that the interfacial spins of Co(1)/$Ir_{25}Mn_{75}$(4) can be switched by SOT.[28] The R_H vs H_z loops, obtained after applying different single current pulses in $H_x = 1$ kOe, are displayed in Fig. S1 in the supplementary material.

Furthermore, utilizing a single pulse of 40 mA under $H_z = 2$ kOe generates a single-step R_H vs H_z loop with positive EB [Fig. 1(e)], suggesting a complete alignment of the interfacial spins of Co(1)/$Ir_{25}Mn_{75}$(4) in the direction of H_z. Strikingly, the R_H vs H_z loop indeed displays an obviously vertical magnetization shift (VMS) as we expect, which is not observed for the device after applying I_p in H_x [Figs. 1(c) and 1(d)]. The exchange bias field H_E and VMS R_{HE} are marked in Fig. 1(e), and the relative VMS, defined as $|R_{HE}/R_{HS+}|$, reaches about 30% [the R_{HS+} and R_{HS-} are saturated R_H at positive (2200 Oe) and negative (-2200 Oe) fields, respectively], which is much larger than that reported in the conventional field-cooling AFM/FM system.[9–12] As the positive and negative I_p values have nearly the same effect on

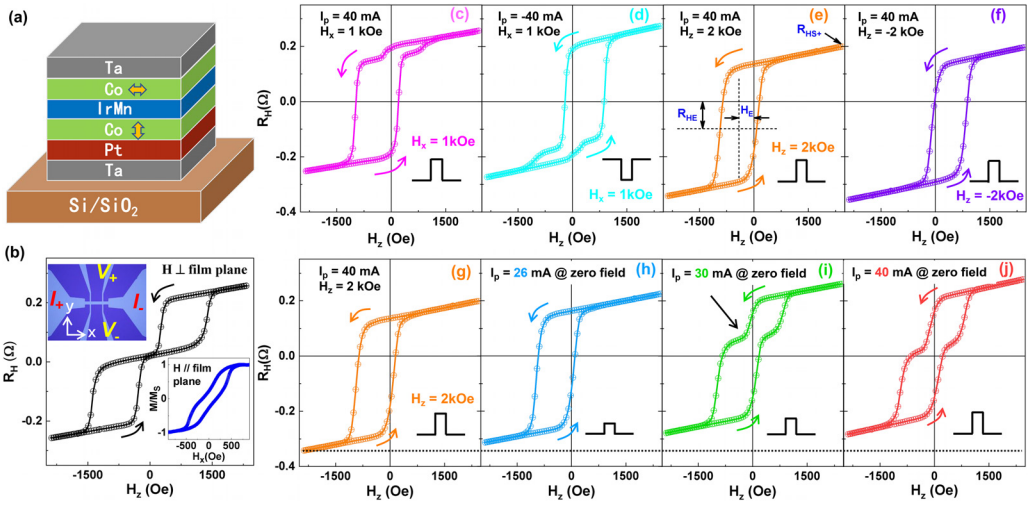

FIG. 1. (a) Schematic of the stack; orange double headed arrows indicate the easy axis of the two ferromagnetic layers. (b) R_H vs H_z curve for sample Ta(1)/Pt(3)/Co(1)/$Ir_{25}Mn_{75}$(4)/Co(5)/Ta(2) before applying current pulses. Inset: (up) optical micrograph of the fabricated Hall device and measurement scheme with the definition of x–y–z coordinates and (down) magnetization hysteresis loop (H//film plane) by a MOKE magnetometer. R_H vs H_z curves after applying a single pulse of 40 mA (c) or -40 mA (d) in $H_x = 1$ kOe. R_H vs H_z curves after utilizing a single pulse of 40 mA in $H_z = 2$ kOe (e) or -2 kOe (f). For the initial state set by applying $I_p = 40$ mA under $H_z = 2$ kOe (g). R_H vs H_z curves were obtained after using each single pulse $I_p = 26$ mA (h), 30 mA (i) and 40 mA (j) in zero field, respectively.

Published under license by AIP Publishing

switching out-of-plane interfacial spins under H_z,[28] we measured the device using a single pulse 40 mA under $H_z = -2$ kOe [Fig. 1(f)], which exhibits a negative EB but the same VMS as that in Fig. 1(e).

As a comparison, the VMS is not observed in the Ta(1)/Pt(3)/Co(1)/$Ir_{25}Mn_{75}$(4)/Ta(2) device (Fig. S2 in the supplementary material). It has been reported that the VMS observed in the FM/AFM system is mainly due to a number of frozen uncompensated or canting AFM spins at the FM/AFM interface.[9–14] For the Ta(1)/Pt(3)/Co(1)/$Ir_{25}Mn_{75}$(4)/Ta(2) device, the interfacial exchange coupling takes place at Co(1)/$Ir_{25}Mn_{75}$(4), and it is very difficult to freeze uncompensated or cant AFM spins in one direction at room temperature.[9–14] However, when covering a top Co layer (for 4 nm $Ir_{25}Mn_{75}$, the interlayer exchange coupling between two FM layers can be ignored.[37]), the interfacial exchange couplings in Co(1)/$Ir_{25}Mn_{75}$(4) (out-of-plane) and in $Ir_{25}Mn_{75}$(4)/Co(5) (in-plane) modify the micromagnetic structure of $Ir_{25}Mn_{75}$.[38] After using I_p under H_z, partial uncompensated AFM spins are pinned in the **z** direction, resulting in the VMS. The same VMS for the device after I_p in positive and negative H_z values would be related to its special AFM microstructure. However, for the device applying I_p under H_x, there is no preferred pinned AFM spins in the **z** direction, and we thus cannot observe the VMS [Figs. 1(c) and 1(d) and S1].

In addition, we found modifications of both EB and VMS induced by SOT in zero field [Figs. 1(h)–1(j)]. The initial state was set by applying a single pulse of 40 mA under $H_z = 2$ kOe [Fig. 1(g)], and subsequent hysteresis loops were obtained after utilizing each single pulse I_p under zero field. For $I_p = 26$ mA, the single-step R_H vs H_z loop moves up [Fig. 1(h)] as compared to the case in Fig. 1(g) (see the dashed line). With increasing I_p to 30 mA, the out-of-plane interfacial spins of Co(1)/$Ir_{25}Mn_{75}$(4) are also varied by SOT, corresponding to a clear step (as the arrow indicates) in the R_H vs H_z loop [Fig. 1(i)]. The switched fraction of out-of-plane interfacial spins, defined as the ratio of the switched R_H step height to the whole loop's height (R_{HS+} - R_{HS-}), is about 30%. When I_p increases to 40 mA, the shape of the two-step R_H vs H_z curve [Fig. 1(j)] becomes similar to the as-deposited condition [Fig. 1(b)].

The relative VMS ($|R_{HE}/R_{HS+}|$) and the switched fraction of out-of-plane interfacial spin dependence of I_p at zero field, starting from an initial state set by applying a single pulse $I_p = 40$ mA under $H_z = 2$ kOe, are summarized in Figs. 2(a) and 2(b), respectively. With increasing I_p from 28 to 32 mA, the $|R_{HE}/R_{HS+}|$ value gradually decreases from 12% to about 0 [Fig. 2(a)], while the switched fraction increases from 3% to the saturated value of 43% [Fig. 2(b)]. Importantly, the $|R_{HE}/R_{HS+}|$ values linearly varies with the switched fraction [Fig. 2(c)].

To understand the field-free SOT-induced variations of EB and VMS, it is needed to consider the effect of the antiferromagnetic domain structure of $Ir_{25}Mn_{75}$. The formation of inequivalent upward and downward domain populations after applying a single pulse of $I_p = 40$ mA under $H_z = 2$ kOe generates an effective out-of-plane field ($H_{z\text{-eff}}$). This can be considered as a training effect, where the built-in $H_{z\text{-eff}}$ helps the SOT to alter the out-of-plane interfacial spins from a metastable domain state to an equilibrium state, corresponding to the orientation of interfacial spins from one direction to nearly equal weighting of its upper and lower parts, as shown in the bottom part of Fig. 2 in Ref. 28. In this process, the larger I_p induces more interfacial spins reorientation, generating the decrease in $H_{z\text{-eff}}$. This leads to the

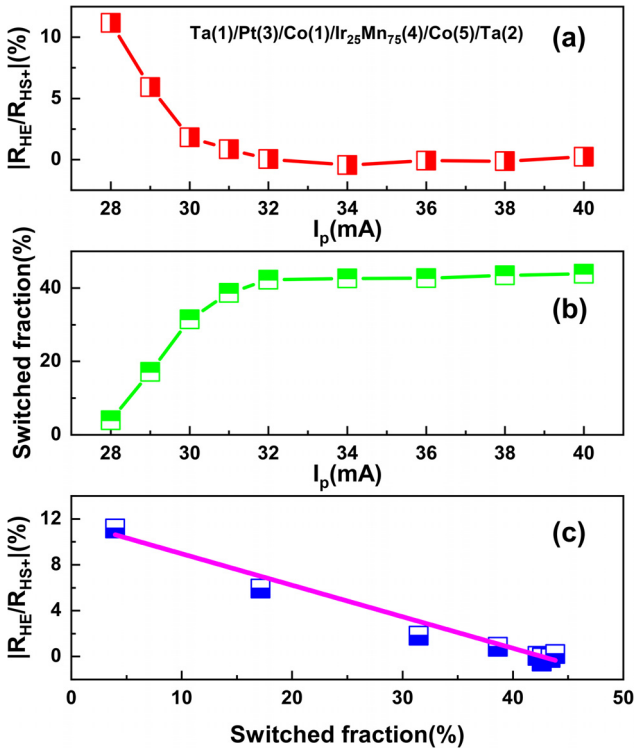

FIG. 2. (a) The relative VMS $|R_{HE}/R_{HS+}|$ and (b) the switched fraction of out-of-plane interfacial spins vs pulsed current. (c) $|R_{HE}/R_{HS+}|$ linearly varies with the switched fraction.

reduction of VMS and the increase in the switched fraction of interfacial spins [Fig. 2(c)]. Here, it is found that the frozen AFM spins depend on $H_{z\text{-eff}}$. As $H_{z\text{-eff}}$ disappears for the equilibrium state, the out-of-plane interfacial spins could not be modified by SOT without an external field.[32–35] Therefore, the VMS disappears, and the switched faction of interfacial spins becomes constant, as shown in Figs. 2(a) and 2(b). Importantly, we actually found an efficient way to initialize the interfacial spins via SOT at zero field. Moreover, we excluded the role of Joule heating in the observed EB and VMS (Figs. S3 and S4 in the supplementary material),[39] and the spin current contribution is mainly from Pt (Fig. S5 in the supplementary material).

From the Meiklejohn and Bean model,[1–3] the macroscopic H_E of the fully uncompensated and pinned FM/AFM interface can be written as a function of the unidirectional magnetic interface energy σ and the Heisenberg-like interface exchange energy J

$$H_E = \frac{\sigma}{M_{FM} t_{FM}} = J \frac{S_{AFM} S_{FM}}{a_{AFM}^2 M_{FM} t_{FM}}, \quad (1)$$

where M_{FM} and t_{FM} are the magnetization and thickness of the FM, a_{AFM} is the size of the unit cell of the AFM, and S_{AFM} and S_{FM} are the spins of the interfacial AFM and FM atoms. Since J, M_{FM}, t_{FM}, and a_{AFM} are constant, the variation of H_E associating with the magnetization reversal of the bottom Co by SOT, corresponding to the switched fraction, mainly reveals the change in S_{AFM}. The linear relationship between $|R_{HE}/R_{HS+}|$ and the switched fraction suggests that the

Published under license by AIP Publishing

number of uncompensated pinned AFM spins is inversely proportional to the switched S_{AFM}.[11,12] The maximum (minimum) $|R_{HE}/R_{HS+}|$ corresponds to the minimum (maximum) switched fraction via SOT at zero field [Fig. 2(c)].

To obtain more insights into the control of VMS via SOT in the HM/FM/AFM/FM device, we measured the R_H vs H_z loops using a constant single pulse $I_p = 29$ mA under different H_z values, starting from an initial state set by applying a single pulse 40 mA under $H_z = 2$ kOe [Fig. 3]. Clearly, the changes in both EB and VMS are observed. The $|R_{HE}/R_{HS+}|$ and switched fraction of out-of-plane interfacial spins vs H_z at $I_p = 29$ mA are plotted in Figs. 4(a) and 4(b), respectively. Two distinct behaviors are observed: $|R_{HE}/R_{HS+}|$ slightly decreases with enhancing H_z from −10 Oe and reaches a minimum of 5% for −200 Oe, and then, this value gradually increases to about 30% for −2000 Oe. Correspondingly, the switched fraction sharply increases from 26% for −10 Oe to 80% for −200 Oe and then slightly increases to 100% with further increasing H_z.

It is noteworthy that the curves in Figs. 4(a) and 4(b) can be divided into two parts, as the dashed line indicates $H_z = -200$ Oe. The linear variation of $|R_{HE}/R_{HS+}|$ with the switched fraction exhibits the opposite sign of the slope for these two parts [Figs. 4(c) and 4(d)]. Unlike the zero field case, the VMS always exists for all the H_z range [Fig. 4(a)]. In this process, both the external field H_z and built-in $H_{z\text{-eff}}$ involve in the variation of $|R_{HE}/R_{HS+}|$ and switched fraction, but H_z plays a dominant role. For $|H_z| < 200$ Oe, the trend of $|R_{HE}/R_{HS+}|$ with the switched fraction is similar to the zero field case. Here, H_z involves the following two steps: (i) assists the out-of-plane interfacial spins for rapid switching and (ii) prevents the full relaxation of uncompensated pinned spins to zero, through SOT. When $|H_z| > 200$ Oe, a slight enhancement of the switched fraction leads to a great increase in $|R_{HE}/R_{HS+}|$. Accordingly, the larger H_z induces more uncompensated out-of-plane pinned spins via SOT.

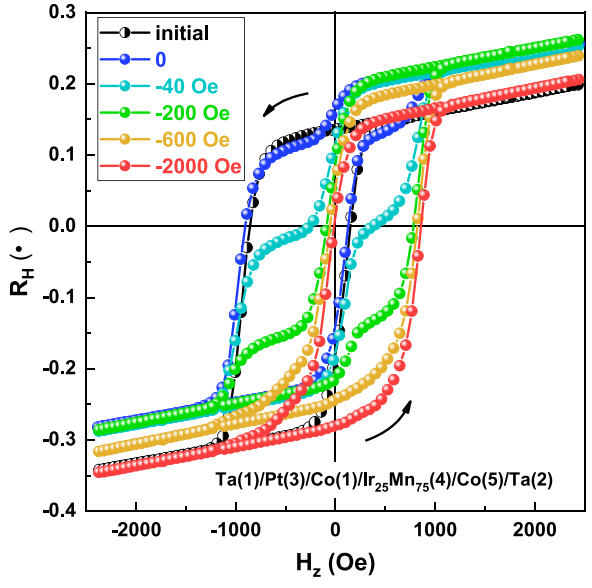

FIG. 3. R_H vs H_z curves after applying a single current pulse $I_p = 29$ mA under different H_z values (0, −40, −200, −600, and −2000 Oe).

The formation of the two regions separated at $H_z = -200$ Oe in Fig. 4(a) would be related to the AFM domain structure of $Ir_{25}Mn_{75}$. For our Pt/Co/$Ir_{25}Mn_{75}$/Co device, partial AFM domains would not move toward **z**, which induces the pinning of a part of the interfacial spins in directions deviated from the **z** direction.[28] The interfacial spins with effective spin moments along in-plane cannot be changed to the **z** direction via SOT under H_x [see a clear step in R_H vs H_z curves in Figs. 1(c) and 1(d)]. However, the SOT under large H_z can flip all the spins to the **z** direction with the help of a strong Zeeman interaction. $H_{z\text{-eff}}$ increases, and thus, more frozen AFM spins are formed, and hence, the sharp increase in $|R_{HE}/R_{HS+}|$ in $|H_z| > 200$ Oe might be due to the rotation of in-plane pinning by $Ir_{25}Mn_{75}$ domains to the **z** direction. Therefore, we implemented the control of VMS and EB via SOT in the Pt/Co/$Ir_{25}Mn_{75}$/Co heterostructure.

In conclusion, we studied the manipulation of VMS and EB through SOT in the Pt(3)/Co(1)/$Ir_{25}Mn_{75}$(4)/Co(5) heterostructure device. The current-induced EB with a large relative VMS of about 30% is found. Furthermore, the field-free SOT-induced variations of VMS and EB is also observed, which would be associated with the effective built-in $H_{z\text{-eff}}$ due to unequal upward and downward interfacial spin populations. We demonstrated an effective way to initialize the interfacial spins through SOT at zero field. The linear relationship between the switched fraction of out-of-plane interfacial spins with $|R_{HE}/R_{HS+}|$ reveals that the number of uncompensated pinned spins is proportional to the switched interfacial spins by SOT. Our work would

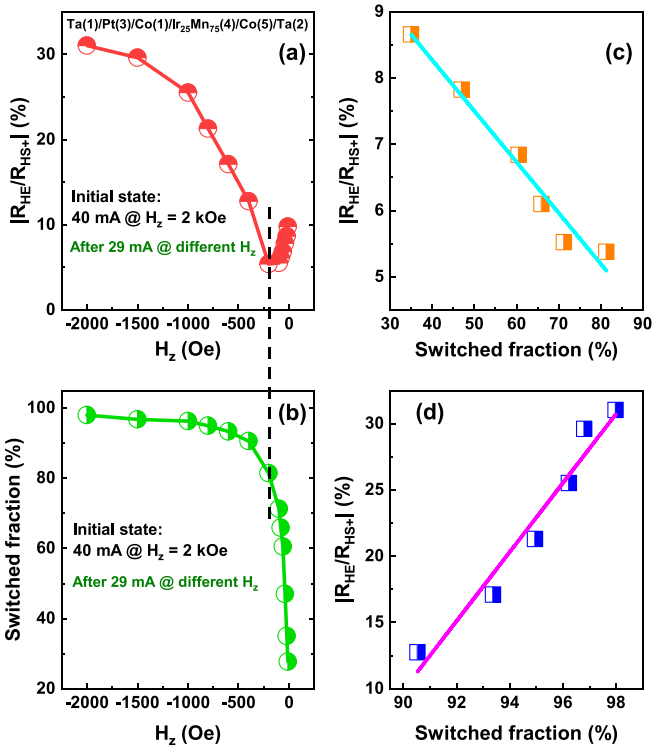

FIG. 4. (a) The relative VMS $|R_{HE}/R_{HS+}|$ and (b) the switched fraction of out-of-plane interfacial spins vs H_z. (c) and (d) The linear relationship between $|R_{HE}/R_{HS+}|$ and the switched fraction of out-of-plane interfacial spins for the two H_z ranges separated by the dashed line in (a) and (b).

Published under license by AIP Publishing

be very important for understanding and utilizing the AFM interfacial spins in related spintronic applications.

See the supplementary material for EB change by different single pulses in $H_x = 1$ kOe for device Ta(1)/Pt(3)/Co(1)/$Ir_{25}Mn_{75}$(4)/Co(5)/Ta(2), EB change by a single pulse $I_p = 26$ mA in $H_z = \pm 2$ kOe for sample Ta(1)/Pt(3)/Co(1)/$Ir_{25}Mn_{75}$(4)/Ta(2), determinations of the temperature increase due to Joule heating during the single current pulse and the blocking temperature of the $Ir_{25}Mn_{75}$ layer for sample Ta(1)/Pt(3)/Co(1)/$Ir_{25}Mn_{75}$(4)/Ta(2), and the variation of EB by SOT in Ta(1)/Pt(3)/Co(1)/$Ir_{25}Mn_{75}$(4)/Co(5)/Al_2O_3(2) and Ta(1)/Pt(3)/Co(1.2)/$Ir_{25}Mn_{75}$(4)/Ru(3) devices.

This work was supported by the National Key R&D Program of China No. 2017YFB0405700. This work was also supported by the NSFC Grant Nos. 11474272 and 61774144 and Beijing Natural Science Foundation Key Program Grant No. Z190007. The Project was sponsored by the Chinese Academy of Sciences, Grant Nos. QYZDY-SSW-JSC020, XDB28000000, and XDPB12 as well.

REFERENCES

[1]W. H. Meiklejohn and C. P. Bean, Phys. Rev. **102**, 1413 (1956).
[2]A. E. Berkowitz and K. Takano, J. Magn. Magn. Mater. **200**, 552 (1999).
[3]J. Nogues, J. Sort, V. Langlais, V. Skumryev, S. Surinach, J. S. Munoz, and M. D. Baro, Phys. Rep. **422**, 65 (2005).
[4]A. R. Ball, A. J. G. Leenaers, P. J. van der Zaag, K. A. Shaw, B. Singer, D. M. Lind, H. Frederikze, and M. T. Rekveldt, Appl. Phys. Lett. **69**, 1489 (1996).
[5]M. Ali, C. H. Marrows, and B. J. Hickey, Phys. Rev. B **67**, 172405 (2003).
[6]X. H. Liu, W. Liu, Z. D. Zhang, and C. F. Chang, J. Appl. Phys. **123**, 083903 (2018).
[7]S. Bhatti, R. Sbiaa, A. Hirohata, H. Ohno, S. Fukami, and S. N. Piramanayagam, Mater. Today **20**, 530 (2017).
[8]M. Gruyters and D. Schmitz, Phys. Rev. Lett. **100**, 077205 (2008).
[9]J. Nogues, C. Leighton, and I. K. Schuller, Phys. Rev. B **61**, 1315 (2000).
[10]H. Ohldag, A. Scholl, F. Nolting, E. Arenholz, S. Maat, A. T. Young, M. Carey, and J. Stohr, Phys. Rev. Lett. **91**, 017203 (2003).
[11]P. H. Huang, H. H. Huang, and C. H. Lai, Appl. Phys. Lett. **90**, 062509 (2007).
[12]Z. M. Tian, S. L. Yuan, S. Y. Yin, L. Liu, J. H. He, H. N. Duan, P. Li, and C. H. Wang, Appl. Phys. Lett. **93**, 222505 (2008).
[13]J. de la Venta, M. Erekhinsky, S. Wang, K. G. West, R. Morales, and I. K. Schuller, Phys. Rev. B **85**, 134447 (2012).
[14]S. J. Yuan, L. Li, T. F. Qi, L. E. DeLong, and G. Cao, Phys. Rev. B **88**, 024413 (2013).
[15]D. Mauri, H. C. Siegmann, and P. S. Bagus, J. Appl. Phys. **62**, 3047 (1987).
[16]K. Takano, R. H. Kodama, A. E. Berkowitz, W. Cao, and G. Thomas, Phys. Rev. Lett. **79**, 1130 (1997).
[17]N. C. Koon, Phys. Rev. Lett. **78**, 4865 (1997).
[18]V. Baltz, A. Manchon, M. Tsoi, T. Moriyama, T. Ono, and Y. Tserkovnyak, Rev. Mod. Phys. **90**, 015005 (2018).
[19]A. Manchon, J. Zelezny, I. M. Miron, T. Jungwirth, J. Sinova, A. Thiaville, K. Garello, and P. Gambardella, Rev. Mod. Phys. **91**, 035004 (2019).
[20]P. Wadley, B. Howells, J. Zelezny, C. Andrews, V. Hills, R. P. Campion, V. Novak, K. Olejnik, F. Maccherozzi, S. S. Dhesi, S. Y. Martin, T. Wagner, J. Wunderlich, F. Freimuth, Y. Mokrousov, J. Kunes, J. S. Chauhan, M. J. Grzybowski, A. W. Rushforth, K. W. Edmonds, B. L. Gallagher, and T. Jungwirth, Science **351**, 587 (2016).
[21]O. Gomonay, T. Jungwirth, and J. Sinova, Phys. Rev. Lett. **117**, 017202 (2016).
[22]K. Olejnik, T. Seifert, Z. Kaspar, V. Novak, P. Wadley, R. P. Campion, M. Baumgartner, P. Gambardella, P. Nemec, J. Wunderlich, J. Sinova, P. Kuzel, M. Muller, T. Kampfrath, and T. Jungwirth, Sci. Adv. **4**, 3566 (2018).
[23]R. Lebrun, A. Ross, S. A. Bender, A. Qaiumzadeh, L. Baldrati, J. Cramer, A. Brataas, R. A. Duine, and M. Klaui, Nature **561**, 222 (2018).
[24]X. Z. Chen, R. Zarzuela, J. Zhang, C. Song, X. F. Zhou, G. Y. Shi, F. Li, H. A. Zhou, W. J. Jiang, F. Pan, and Y. Tserkovnyak, Phys. Rev. Lett. **120**, 207204 (2018).
[25]I. M. Miron, K. Garello, G. Gaudin, P. J. Zermatten, M. V. Costache, S. Auffret, S. Bandiera, B. Rodmacq, A. Schuhl, and P. Gambardella, Nature **476**, 189 (2011).
[26]L. Q. Liu, C. F. Pai, Y. Li, H. W. Tseng, D. C. Ralph, and R. A. Buhrman, Science **336**, 555 (2012).
[27]P.-H. Lin, B.-Y. Yang, M.-H. Tsai, P.-C. Chen, K.-F. Huang, H.-H. Lin, and C.-H. Lai, Nat. Mater. **18**, 335 (2019).
[28]X. H. Liu, K. W. Edmonds, Z. P. Zhou, and K. Y. Wang, Phys. Rev. Appl. **13**, 014059 (2020).
[29]Y. Sheng, K. W. Edmonds, X. Ma, H. Zheng, and K. Y. Wang, Adv. Electron. Mater. **4**, 1800224 (2018).
[30]S. Brück, J. Sort, V. Baltz, S. Surinach, J. S. Munoz, B. Dieny, M. D. Baro, and J. Nogues, Adv. Mater. **17**, 2978 (2005).
[31]J. Y. Chen, N. Thiyagarajah, H. J. Xu, and J. M. D. Coey, Appl. Phys. Lett. **104**, 152405 (2014).
[32]Y. C. Li, K. W. Edmonds, X. H. Liu, H. Z. Zheng, and K. Y. Wang, Adv. Quantum Technol. **2**, 1800052 (2019).
[33]K. Cai, M. Yang, H. Ju, S. Wang, Y. Ji, B. Li, K. W. Edmonds, Y. Sheng, B. Zhang, N. Zhang, S. Liu, H. Zheng, and K. Y. Wang, Nat. Mater. **16**, 712 (2017).
[34]Y. Cao, A. W. Rushforth, Y. Sheng, H. Zheng, and K. Y. Wang, Adv. Funct. Mater. **29**, 1808104 (2019).
[35]M. Yang, K. Cai, H. Ju, K. W. Edmonds, G. Yang, S. Liu, B. Li, B. Zhang, Y. Sheng, S. Wang, Y. Ji, and K. Y. Wang, Sci. Rep. **6**, 20778 (2016).
[36]A. Ghosh, S. Auffret, U. Ebels, and W. E. Bailey, Phys. Rev. Lett. **109**, 127202 (2012).
[37]S. S. Parkin, Phys. Rev. Lett. **67**, 3598 (1991).
[38]Y. Y. Wang, C. Song, G. Wang, J. Miao, F. Zeng, and F. Pan, Adv. Funct. Mater. **24**, 6806 (2014).
[39]C. C. Chiang, S. Y. Huang, D. Qu, P. H. Wu, and C. L. Chien, Phys. Rev. Lett. **123**, 227203 (2019).

Published under license by AIP Publishing